ZEUS-prel-06-023

Submitted to the
33nd International Conference on High Energy Physics
July 26 – August 2, 2006; Moscow, Russia

Session: QCD hard interactions

Multijet production at low-x in deep inelastic scattering at HERA

ZEUS Collaboration

24th July 2006

Abstract

Di- and trijet production in deep inelastic ep scattering has been measured with an integrated luminosity of 82.2 pb^{-1} for $10 < Q^2 < 100$ GeV^2 in the region of small Bjorken x ($10^{-4} < x_{\rm Bj} < 10^{-2}$) and compared to the predictions based on next-to-leading-order QCD calculations.

1 Introduction

Multijet production in deep inelastic scattering (DIS) at HERA [1, 2] has been used to test the predictions of perturbative QCD (pQCD) over a large range of four-momentum transfer squared, Q^2, and to determine the strong coupling constant α_s. At leading order (LO) in α_s, dijet production in neutral current DIS proceeds via the boson-gluon-fusion (BGF, $V^*g \rightarrow q\bar{q}$ with $V = \gamma$, Z^0) and QCD-Compton (QCDC, $V^*q \rightarrow qg$) processes. Events with three jets can be seen as dijet processes with an additional gluon radiation or splitting of a gluon into a quark-antiquark pair and are directly sensitive to $\mathcal{O}(\alpha_s^2)$ QCD effects. The higher sensitivity to α_s and the large number of degrees of freedom of the trijet final state provide tests of the QCD predictions.

Recent H1 studies [3] compared multi-differential cross sections with NLO QCD DGLAP-based predictions in the low-Q^2 and low-x_{Bj} region. Reasonable agreement between data and the theoretical calculations was found, except for the azimuthal correlation between jets, where the NLO QCD predictions failed to describe the data.

In this analysis, the multi-differential cross sections and angular jet correlations for dijet and trijet production in the hadronic center-of-mass (HCM) frame are measured with high statistical precision in the kinematic region defined by $10 < Q^2 < 100\,\mathrm{GeV}^2$ and $0.0001 < x_{\mathrm{Bj}} < 0.01$. The results are compared with pQCD calculations at next-to-leading order (NLO).

2 Kinematics and event selection

The results presented in this paper correspond to an integrated luminosity of 82.2 ± 2.0 pb^{-1} taken with the ZEUS detector during the 1998-2000 HERA running period. Positrons or electrons[1] of energy $E_e = 27.5$ GeV collided with protons of energy $E_p = 920$ GeV, giving a center of mass energy $\sqrt{s} = 318$ GeV.

A detailed description of the ZEUS detector can be found elsewhere [4,5]. Neutral current DIS events were selected by requiring that a scattered electron candidate with an energy more than 4 GeV was measured in the uranium-scintillator calorimeter (CAL) [6]. The Bjorken scaling variable x_{Bj}, the inelasticity y, and Q^2 were reconstructed offline using the electron and Jacquet-Blondel [7](JB) methods. The offline selection of DIS events was similar to that used in a previous ZEUS measurement [1] and was based on the following requirements:

[1] In the following, the term "electron" denotes generically both the electron (e^-) and the positron (e^+).

- y_e<0.7, where y_e is y as reconstructed by the electron method, to reduce the photoproduction background and place an implicit cut on the energy of the scattered electron;
- $y_{\rm JB}$>0.1, where $y_{\rm JB}$ is y reconstructed by the JB method;
- $40<\delta<60\,{\rm GeV}$, where $\delta = \sum_i (E-P_Z)_i$ and the sum runs over all energy deposits. The lower cut removed background from photoproduction and events with large initial-state QED radiation. The upper cut removed cosmic-ray background;
- $|Z_{\rm vtx}|$<50 cm, where $Z_{\rm vtx}$ is the Z position of the reconstructed primary vertex, to select events consistent with ep collisions.

The kinematic range of the analysis is:

$$10 < Q^2 < 100\,{\rm GeV}^2,\ 10^{-4} < x_{\rm Bj} < 10^{-2} \text{ and } 0.1 < y < 0.7.$$

For each event, the reconstruction of the kinematic variables and jets was performed using a combination of track and CAL information, excluding the cells and the track associated with the scattered electron. The selected tracks and CAL clusters were treated as massless Energy Flow Objects (EFOs) [8]. The minimum transverse momentum, p_T, of each EFO was required to be greater than 0.15 GeV.

Jets were reconstructed using the k_T cluster algorithm [9] in the longitudinally invariant inclusive mode [10]. The jet search was conducted in the hadronic center-of-mass (HCM) frame.

The jet phase space is defined by selection cuts on the jet pseudorapidity, $\eta^{\rm jet}_{\rm LAB}$, in the laboratory frame and on the jet transverse energy, $E^{\rm jet}_{T,HCM}$, in the HCM frame:

$$-1.0 < \eta^{\rm jet1,2,(3)}_{\rm LAB} < 2.5 \text{ and } E^{\rm jet1}_{T,HCM} > 7, E^{\rm jet2,(3)}_{T,HCM} > 5 \text{ GeV},$$

where jet1,2,(3) referred to the two (three) jets with the highest transverse energy in the HCM frame of a given event.

3 Monte Carlo simulation

Monte Carlo (MC) simulations were used to correct the data for detector effects, inefficiencies of the event selection and that of the jet reconstruction, as well as for QED effects. Neutral current DIS events were generated using the ARIADNE 4.10 program [11] and the LEPTO 6.5 program [12] interfaced to HERACLES 4.5.2 [13] via DJANGO 6.2.4 [14]. The HERACLES program includes QED effects up to $\mathcal{O}(\alpha^2_{\rm EM})$. In case of ARIADNE, the QCD cascade is simulated using the colour-dipole model [15], whereas for LEPTO, the matrix elements plus parton shower model is used. For hadronization both models use the Lund string model [16], as implemented in JETSET 7.4 [17, 18].

The ZEUS detector response was simulated with a program based on GEANT 3.13 [19]. The generated events were passed through the detector simulation, subjected to the same trigger requirements as the data, and processed by the same reconstruction and offline programs.

Measured distributions of kinematic variables are well described by both the ARIADNE and LEPTO MC models after reweighting in Q^2 [1]. The LEPTO simulation gives a better overall description of the jet variables, but ARIADNE provides a better description of dijets with small azimuthal separation. Therefore, for this analysis, the events generated with the ARIADNE program were used to determine the acceptance corrections. The events generated with LEPTO were used to estimate the uncertainty associated with the treatment of the parton shower.

4 NLO QCD calculations

The NLO calculations were carried out in the $\overline{\mathrm{MS}}$ scheme for five massless quark flavors with the program NLOJET [20]. NLOJET allows a computation of the dijet (trijet) production cross sections to next-to-leading order, i.e. including all terms up to $\mathcal{O}(\alpha_s^2)$ ($\mathcal{O}(\alpha_s^3)$). In certain regions of the jet phase space, NLOJET provides calculations for dijet production at $\mathcal{O}(\alpha_s^3)$. It was checked that the LO and NLO calculations from NLOJET agree with those of DISENT [21] at the 1-2% level for the dijet cross sections [22, 23].

For comparison with the data, the CTEQ6 [24] parameterisations of the proton parton density functions (PDFs) were used and the renormalisation and factorisation scales were both chosen to be $(\bar{E}_T^2 + Q^2)/4$, where for dijets (trijets) $\bar{E}_T$ is the average E_T of the two (three) highest E_T jets in a given event. The strong coupling constant was set to the value used for the CTEQ6 PDFs, $\alpha_s(M_Z) = 0.118$, and evolved according to the two-loop solution of the renormalisation group equation.

The NLO QCD predictions were corrected for hadronisation effects using a bin-by-bin procedure. Hadronisation correction factors were defined for each bin as the ratio of the hadron- to parton-level cross sections and were calculated using the LEPTO MC program. The correction factors C_{had} were typically in the range $0.8 - 0.9$ for most of the phase space.

5 Results

5.1 Single differential cross sections $d\sigma/dQ^2$, $d\sigma/dx_{\mathrm{Bj}}$ and trijet to dijet cross-section ratios

The single differential cross sections $d\sigma/dQ^2$ and $d\sigma/x_{\mathrm{Bj}}$ for dijet and trijet productions are shown in Figs. 1(a) and (c). The measured dijet and trijet cross sections are well described by the NLOJET calculations.

The cross-section ratio $\sigma_{trijet}/\sigma_{dijet}$ of the trijet cross section to the dijet cross section, in which the experimental and theoretical uncertainties partially cancel, have been used to test the pQCD calculations more precisely than is possible with the individual cross sections. The measurements of the cross section ratio as a function of Q^2 and of x_{Bj} are presented in Figs. 1(b) and 1(d), respectively. The cross-section ratio $\sigma_{trijet}/\sigma_{dijet}$ is almost Q^2 independent, as shown in Fig. 1(b), and falls steeply with increasing x_{Bj}, as shown in Fig. 1(d). Both cross section ratios are reasonably described by NLOJET.

5.2 Transverse energy dependencies of cross sections

The single differential cross section $d\sigma/dE^{\mathrm{jet}}_{T,HCM}$ for the two (three) jets with highest $E^{\mathrm{jet}}_{T,HCM}$ are shown in Fig. 2. The measured cross sections are well described by the NLOJET calculations over the whole range in $E^{\mathrm{jet}}_{T,HCM}$ considered.

Correlations in transverse energy of the jets have been investigated by measuring the triply-differential cross sections $d\sigma/dQ^2dx_{\mathrm{Bj}}d\Delta E_T$, where ΔE_T is the difference in transverse energy between the two jets with the highest $E^{\mathrm{jet}}_{T,HCM}$. The measurement was performed in (x_{Bj}, Q^2) bins, which are defined in Table 1 for dijet and trijet production. Figure 3 shows two representative bins for the dijet, (a) and (b), and (c) and (d) for the trijet samples. Since no significant difference in description of the data has been observed for different bins, the following discussion of the comparison of the data with NLOJET is valid for all the (x_{Bj}, Q^2) bins considered.

The NLOJET calculations at $\mathcal{O}(\alpha_s^2)$ do not describe the high-ΔE_T tail of the dijet sample, where the calculations fall below the data. Since these calculations give the lowest-order non-trivial contribution to the cross section in the region $\Delta E_T > 0\,\mathrm{GeV}$, it is necessary to examine if these calculations are affected by large uncertainties from the higher-order terms. A higher-order calculation is possible with NLOJET, if the region $\Delta E_T \sim 0\,\mathrm{GeV}$ is avoided. NLOJET calculations at $\mathcal{O}(\alpha_s^3)$ for the dijet sample have been obtained for the region $\Delta E_T > 4\,\mathrm{GeV}$ and are compared to the data in Figs. 3(a) and 3(b). The inclusion of the next term in the perturbative series in α_s improves the description of the data in the region of moderate ΔE_T, but the calculations still fall below the data at the highest ΔE_T measured point. The NLOJET calculations at $\mathcal{O}(\alpha_s^3)$ for trijet production, which take into account two terms in the perturbative series in α_s, are consistent with the measurements.

5.3 Pseudorapidity distributions

The single-differential cross section $d\sigma/d\eta^{\rm jet}_{LAB}$ for dijet and trijet production are shown in Figs. 4(a) and 4(c). For this figure, the two (three) jets with highest $E^{\rm jet}_{T,HCM}$ were ordered in $\eta^{\rm jet}_{LAB}$. Also shown are the measurements of the triply-differential cross section $d\sigma/dQ^2dx_{\rm Bj}d|\Delta\eta_{HCM}|$, where $|\Delta\eta_{HCM}|$ is the absolute difference in pseudorapidity of the two jets with highest $E^{\rm jet}_{T,HCM}$ (see Figs 4(b) and 4(d)). NLOJET calculations acceptably describe the measurements.

5.4 Azimuthal distributions of the jets

Measurements of the triply-differential cross section $d\sigma/dQ^2dx_{\rm Bj}d|\Delta\phi_{HCM}|$, where $|\Delta\phi_{HCM}|$ is the absolute difference in azimuth between the two jets with highest $E^{\rm jet}_{T,HCM}$, for dijet and trijet production are shown in Fig. 5 for two representative bins in $(x_{\rm Bj}, Q^2)$. For dijet and trijet production the cross section falls with $|\Delta\phi_{HCM}|$. The NLOJET calculations at $\mathcal{O}(\alpha_S^2)$ for dijet production decrease more rapidly with $|\Delta\phi_{HCM}|$ than the data and the calculations disagree with the data at low $|\Delta\phi_{HCM}|$ (see Fig. 5(a)). Since these calculations give the lowest-order non-trivial contribution to the cross section in the region $|\Delta\phi_{HCM}| < 180°$, it is necessary to examine whether the calculations are affected by large uncertainties due to the higher-order terms. A higher-order calculation is possible with NLOJET provided that the region $|\Delta\phi_{HCM}| \sim 180°$ is avoided. NLOJET calculations at $\mathcal{O}(\alpha_S^3)$ for the dijet sample have been obtained for the region $|\Delta\phi_{HCM}| < 135°$ and describe the data well, see Figs. 5(a) and 5(b). Thus, a good description of the distribution in the azimuthal separation of dijet production has been achieved by including higher-order effects. The measurements for trijet production are reasonably well described by the the NLOJET calculations at $\mathcal{O}(\alpha_S^3)$, which include QCD corrections to the lowest-order contribution.

The cross section $d\sigma/dQ^2dx_{\rm Bj}$ for dijet (trijet) events with $|\Delta\phi_{HCM}| < 120°$ as a function of $x_{\rm Bj}$ are presented in Fig. 6. The cross sections are measured in bins of Q^2. NLOJET calculations at $\mathcal{O}(\alpha_S^2)$ for dijet production underestimate the data, the difference increasing towards low $x_{\rm Bj}$. NLOJET calculations at $\mathcal{O}(\alpha_S^3)$ are consistent with the data, demonstrating the importance of the higher-order terms in the description of the data at low $x_{\rm Bj}$, where they give rise to an increase of about one order of magnitude. This large increase due to the QCD corrections, together with the large dependence on the renormalisation scale, indicates that missing higher-order terms are important in this region. The measurements for trijet production are consistent with the NLOJET calculations at $\mathcal{O}(\alpha_S^3)$ within the large renormalisation scale uncertainties.

6 Summary

Di- and trijet production in deep inelastic ep scattering has been measured for $10 < Q^2 < 100$ GeV^2 in the region of small Bjorken $x_{\rm Bj}$ ($10^{-4} < x_{\rm Bj} < 10^{-2}$) using an integrated luminosity of 82.2 pb^{-1} collected by the ZEUS experiment. The high statistics available have made possible detailed studies of multijet production at low $x_{\rm Bj}$. The dependence of dijet and trijet production on the kinematic variables Q^2 and $x_{\rm Bj}$ and on the jet variables $E_{T,HCM}^{\rm jet}$ and $\eta_{LAB}^{\rm jet}$ is well described by perturbative QCD calculations which include next-to-lowest-order corrections. To investigate possible deviations with respect to the collinear factorization approximation used in the standard pQCD approach, measurements of the correlations between the two jets with highest $E_{T,HCM}^{\rm jet}$ have been made. Measurements of dijet production with low azimuthal separation are reproduced by the perturbative QCD calculations provided that higher-order terms ($\mathcal{O}(\alpha_s^3)$) are accounted for. Such terms increase the predictions of pQCD calculations by about one order of magnitude when the two jets with the highest $E_{T,HCM}^{\rm jet}$ are not strongly correlated in $\phi_{HCM}^{\rm jet}$, thus demonstrating their importance in the region of low $x_{\rm Bj}$. These calculations also improve the description of the distribution of ΔE_T in the data, but underestimate the data at the highest ΔE_T measured point. pQCD calculations of the correlations in trijet production are consistent with the measurements.

Acknowledgements

It is a pleasure to thank the DESY Directorate for their strong support and encouragement. The remarkable achievements of the HERA machine group were essential for the successful completion of this work and are greatly appreciated. The design, construction and installation of the ZEUS detector has been made possible by the efforts of many people who are not listed as authors.

References

[1] ZEUS Coll., S. Chekanov et al., Eur. Phys. J. **C 44**, 183 (2005).

[2] H1 Coll., Adloff, C. et al., Phys. Lett. **B515**, 17 (2001).

[3] H1 Coll., A. Aktas et al., Eur. Phys. J. **C 33**, 477 (2004).

[4] ZEUS Coll., U. Holm (ed.), *The ZEUS Detector*. Status Report (unpublished), DESY (1993), available on `http://www-zeus.desy.de/bluebook/bluebook.html`.

[5] ZEUS Coll., Derrick, M. et al., Phys. Lett. **B293**, 465 (1992).

[6] ZEUS Coll., J. Breitweg et al., Eur. Phys. J. **C 11**, 427 (1999).

[7] F. Jacquet and A. Blondel, *Proceedings of the Study for an ep Facility for Europe*, U. Amaldi (ed.), p. 391. Hamburg, Germany (1979). Also in preprint DESY 79/48.

[8] G.M. Briskin, *Diffractive Dissociation in ep Deep Inelastic Scattering*. Ph.D. Thesis, Tel Aviv University, 1998. DESY-THESIS-1998-036.

[9] S. Catani et al., Nucl. Phys. **B 406**, 187 (1993).

[10] S.D. Ellis and D.E. Soper, Phys. Rev. **D 48**, 3160 (1993).

[11] L. Lönnblad, Comp. Phys. Comm. **71**, 15 (1992).

[12] G. Ingelman, A. Edin and J. Rathsman, Comp. Phys. Comm. **101**, 108 (1997).

[13] A. Kwiatkowski, H. Spiesberger and H.-J. Möhring, Comp. Phys. Comm. **69**, 155 (1992). Also in *Proc. Workshop Physics at HERA*, 1991, DESY, Hamburg.

[14] K. Charchula, G.A. Schuler and H. Spiesberger, Comp. Phys. Comm. **81**, 381 (1994).

[15] G. Gusafson and U. Pettersson, Nucl. Phys. **B 306**, 746 (1988).

[16] B. Andersson et al., Phys. Rep. **97**, 31 (1983).

[17] M. Bengtsson and T. Sjöstrand, Comp. Phys. Comm. **46**, 43 (1987).

[18] T. Sjöstrand, Comp. Phys. Comm. **82**, 74 (1994).

[19] R. Brun et al., GEANT3, Technical Report CERN-DD/EE/84-1, CERN, 1987.

[20] Z. Nagy and Z Trocsanyi, Phys. Rev. Lett. **87**, 082001 (2001).

[21] S. Catani and M. H. Seymour, Nucl. Phys. **B 485**, 291 (1997).

[22] N. Krumnack, *Three Jet Events in Deep Inelastic Scattering*. Thesis, University of Hamburg, 2004.

[23] L. Li, *Multijets in Neutral Current Deep Inelastic Scattering at HERA*. Ph.D. Thesis, University of Wisconsin-Madison, 2004. In preparation.

[24] Pumplin, J. et al., JHEP **07**, 012 (2002).

Bin	Q^2 (GeV^2)	x_{Bj}
1	$10 - 30$	$0.00017 - 0.0003$
2	$10 - 30$	$0.0003 - 0.0005$
3	$10 - 30$	$0.0005 - 0.001$
4	$10 - 30$	$0.001 - 0.0033$
5	$30 - 100$	$0.0005 - 0.001$
6	$30 - 100$	$0.001 - 0.01$

Table 1: *The kinematic boundaries of the bins in* x_{Bj} *and* Q^2.

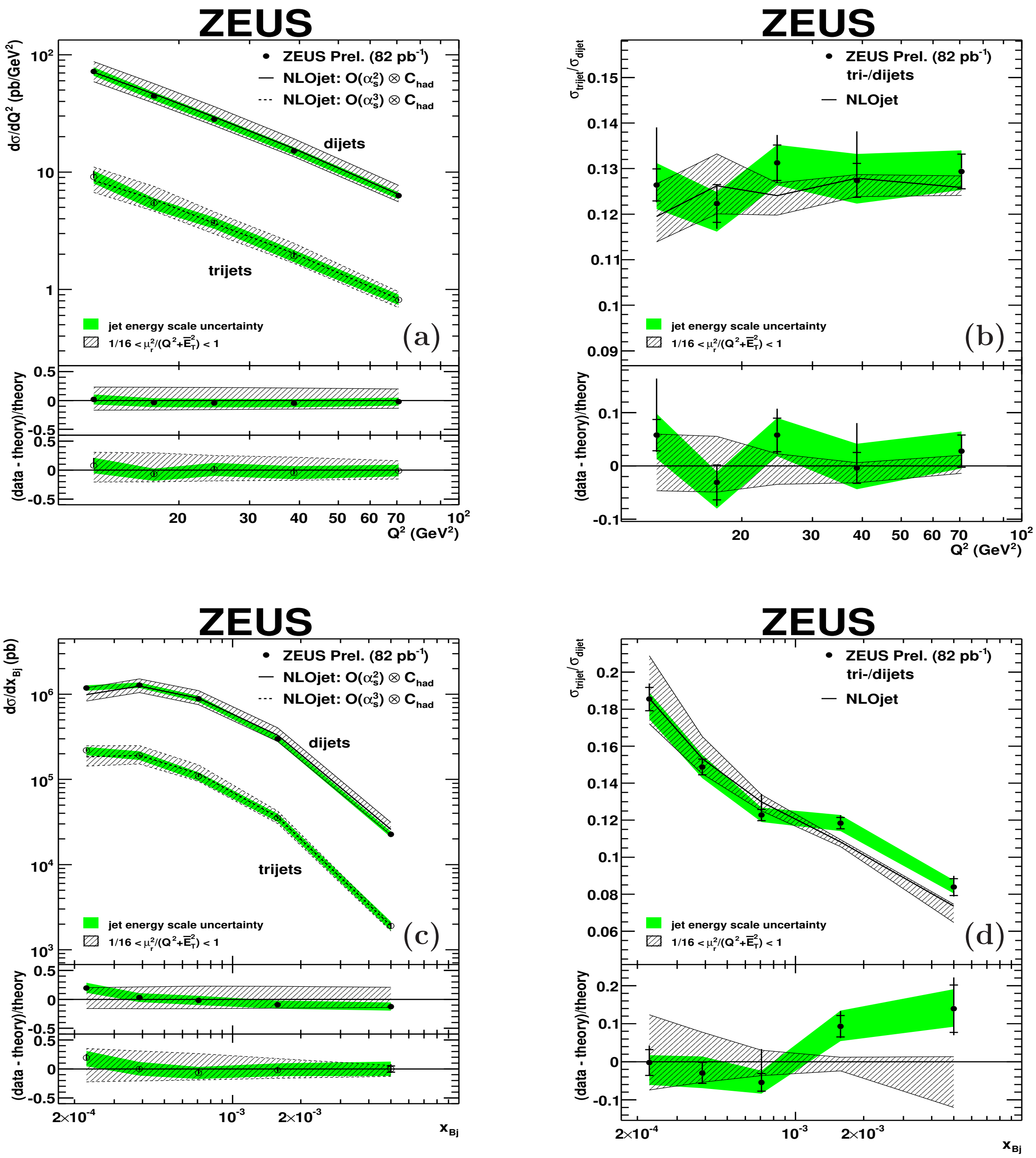

Figure 1: *The inclusive dijet and trijet cross sections as functions of Q^2 and x_{Bj}. (b) and (d) show the ratios of the trijet and dijet cross sections. The inner error bars represent the statistical uncertainties. The outer error bars represent the quadratic sum of statistical and systematic uncertainties not associated with the jet energy scale. The shaded band indicates the jet energy scale uncertainty. The predictions of perturbative QCD at next-to-leading order, corrected for hadronisation effects and using the CTEQ6 parameterisations of the proton PDFs, are compared to the data. The lower plots show the relative difference between the data and the calculations. The hatched band represents the renormalisation scale uncertainty of the QCD calculation.*

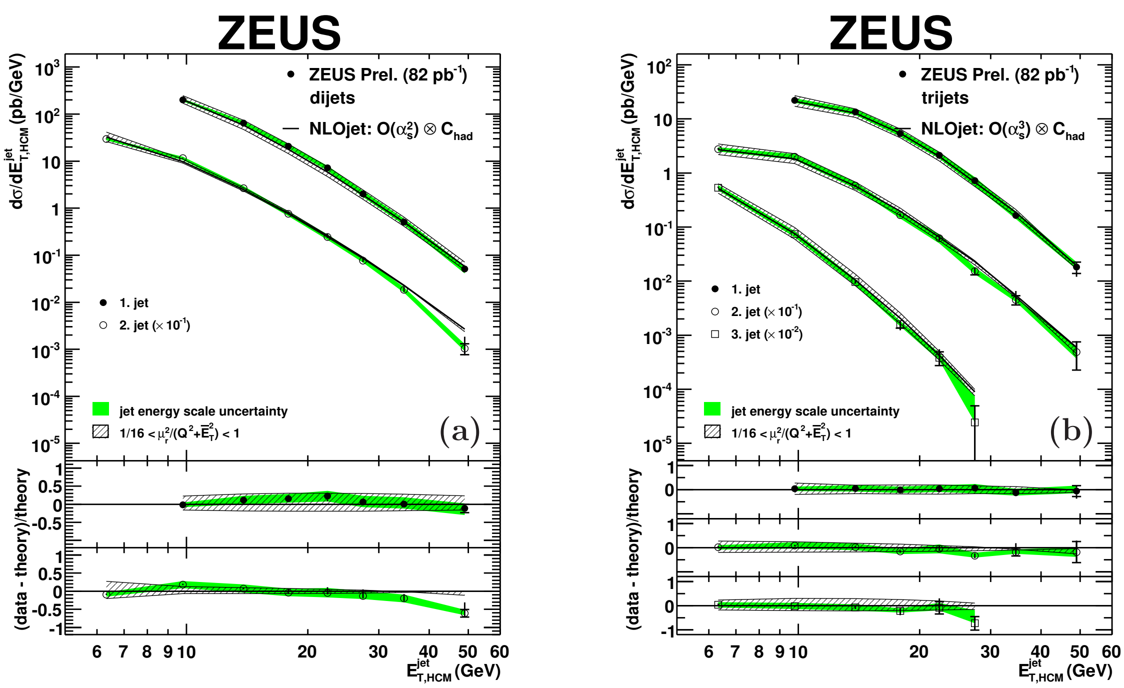

Figure 2: *Inclusive dijet and trijet cross sections as functions of* $E^{\rm jet}_{T,HCM}$ *with the jets ordered in* $E^{\rm jet}_{T,HCM}$*. The cross sections of the second and third jet were scaled for readability. Other details as in the caption to Fig. 1.*

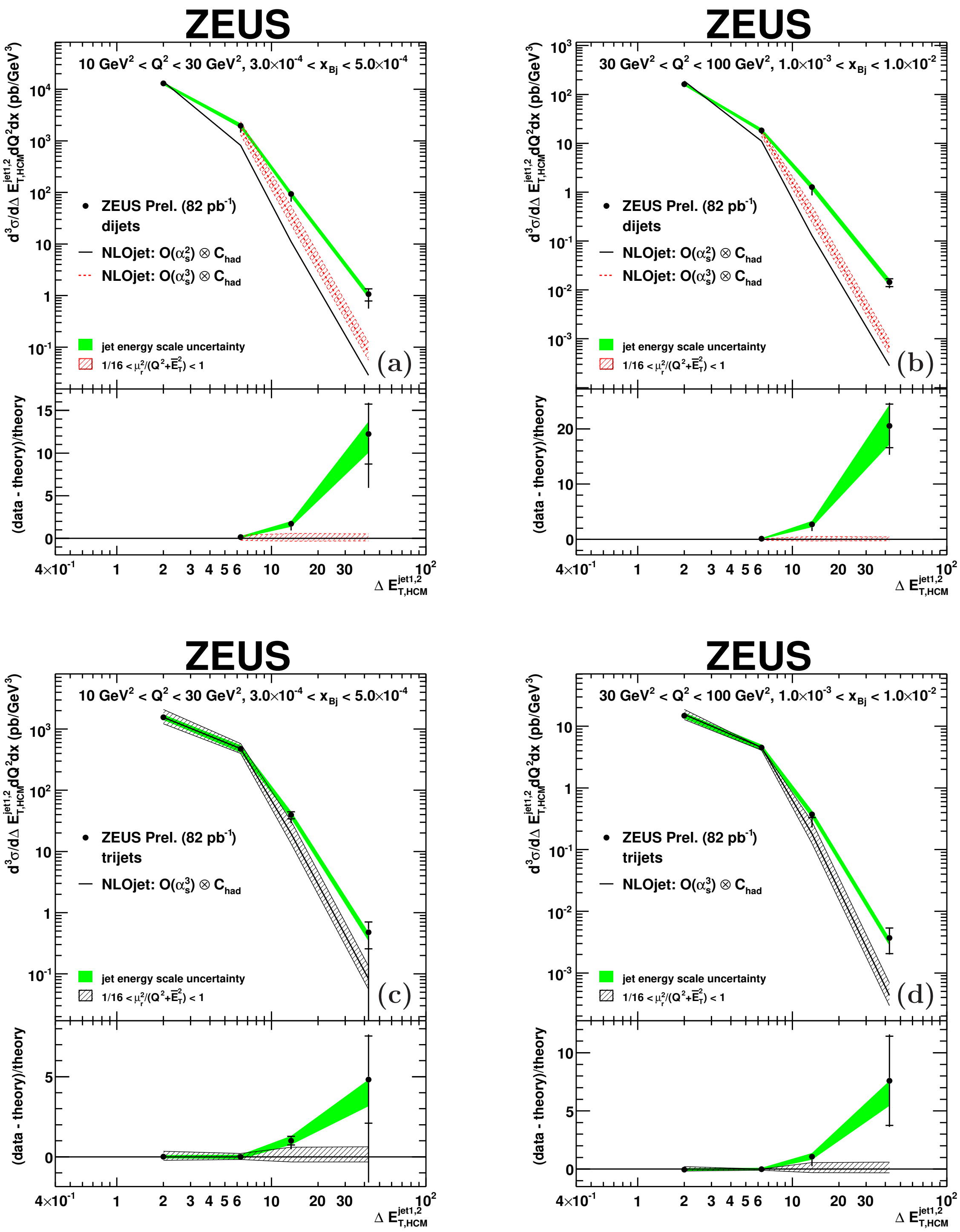

Figure 3: *Dijet and trijet cross sections as functions of $\Delta E_{T,HCM}^{\rm jet1,2}$ in two (x_{Bj}, Q^2)-bins. For comparison with the dijet measurements,* NLOJET *calculations at $\mathcal{O}(\alpha_s^2)$ ($\mathcal{O}(\alpha_s^3)$) are shown as solid (dashed) lines for $\Delta E_{T,HCM} >= 0 \;\; GeV (4 \;\; GeV)$. The trijet measurements are compared to* NLOJET *calculations at $\mathcal{O}(\alpha_s^3)$. Other details as in the caption to Fig. 1.*

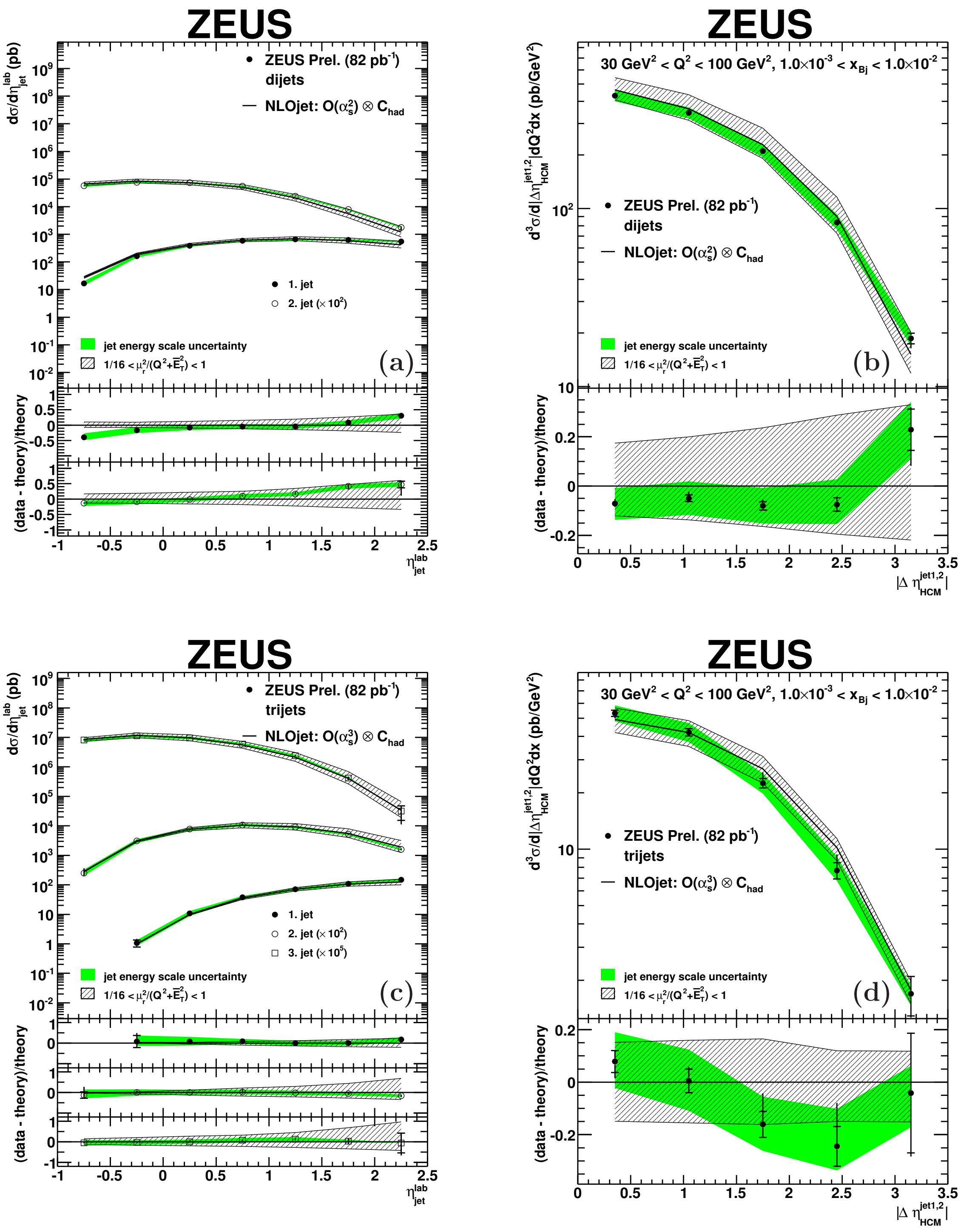

Figure 4: *(a) and (c) show the inclusive dijet and trijet cross sections as functions of $\eta_{LAB}^{\rm jet}$ with the jets ordered in $\eta_{LAB}^{\rm jet}$. The cross sections of the second and third jet were scaled for readability. (b) and (d) show the dijet and trijet cross sections as functions of $\Delta\eta_{HCM}^{\rm jet1,2}$ in one (x_{Bj}, Q^2) bin. Other details as in the caption in Fig. 1.*

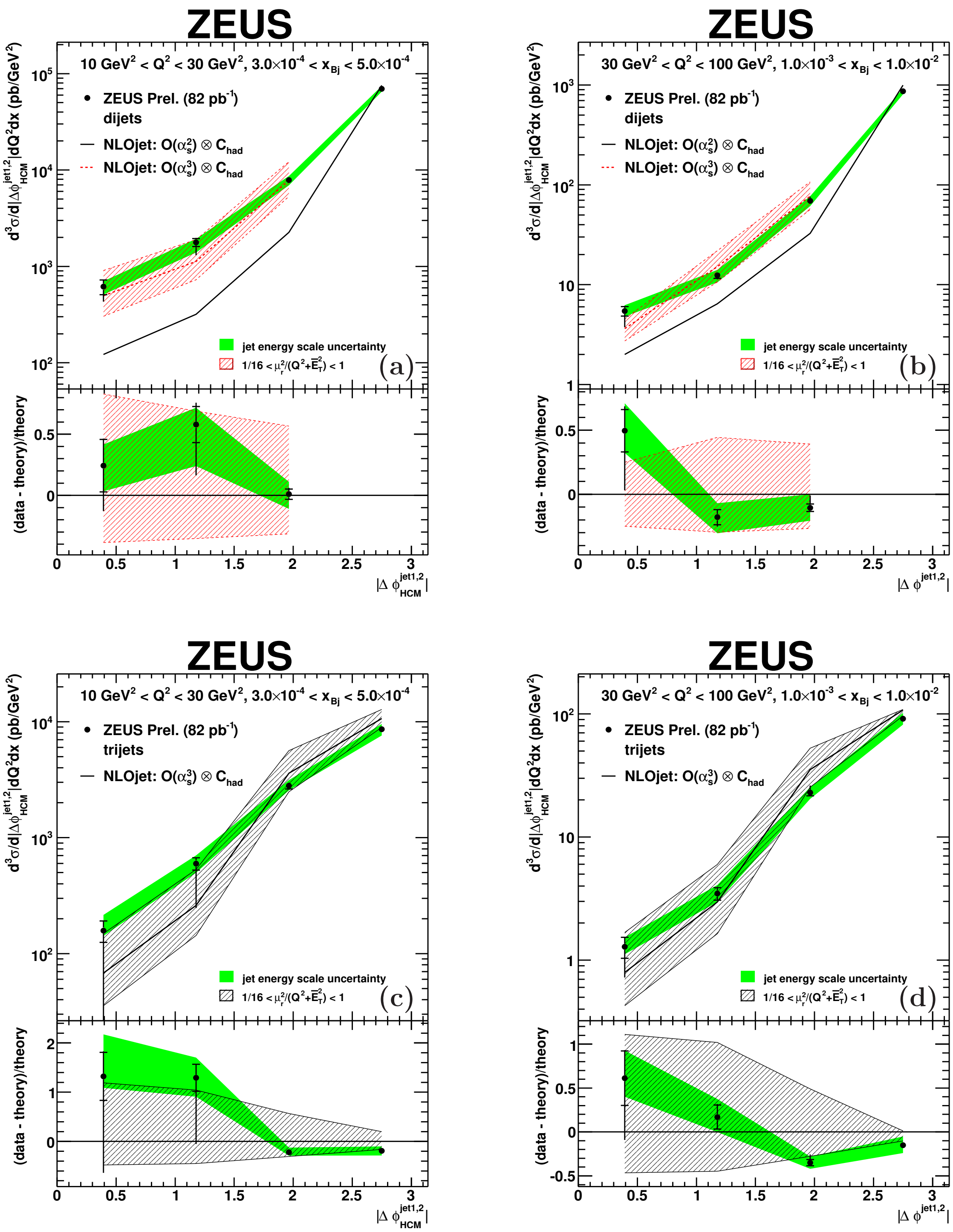

Figure 5: *Dijet and trijet cross sections as functions of $\Delta\phi^{\rm jet1,2}_{HCM}$ in two different (x_{Bj}, Q^2) bins. For comparison with the dijet measurements,* NLOJET *calculations at $\mathcal{O}(\alpha_s^2)$ ($\mathcal{O}(\alpha_s^3)$) are shown as solid (dashed) lines for $\Delta\phi^{\rm jet1,2}_{HCM} <= 180^\circ (135^\circ)$. The trijet measurements are compared to* NLOJET *calculations at $\mathcal{O}(\alpha_s^3)$. Other details as in the caption to Fig. 1.*

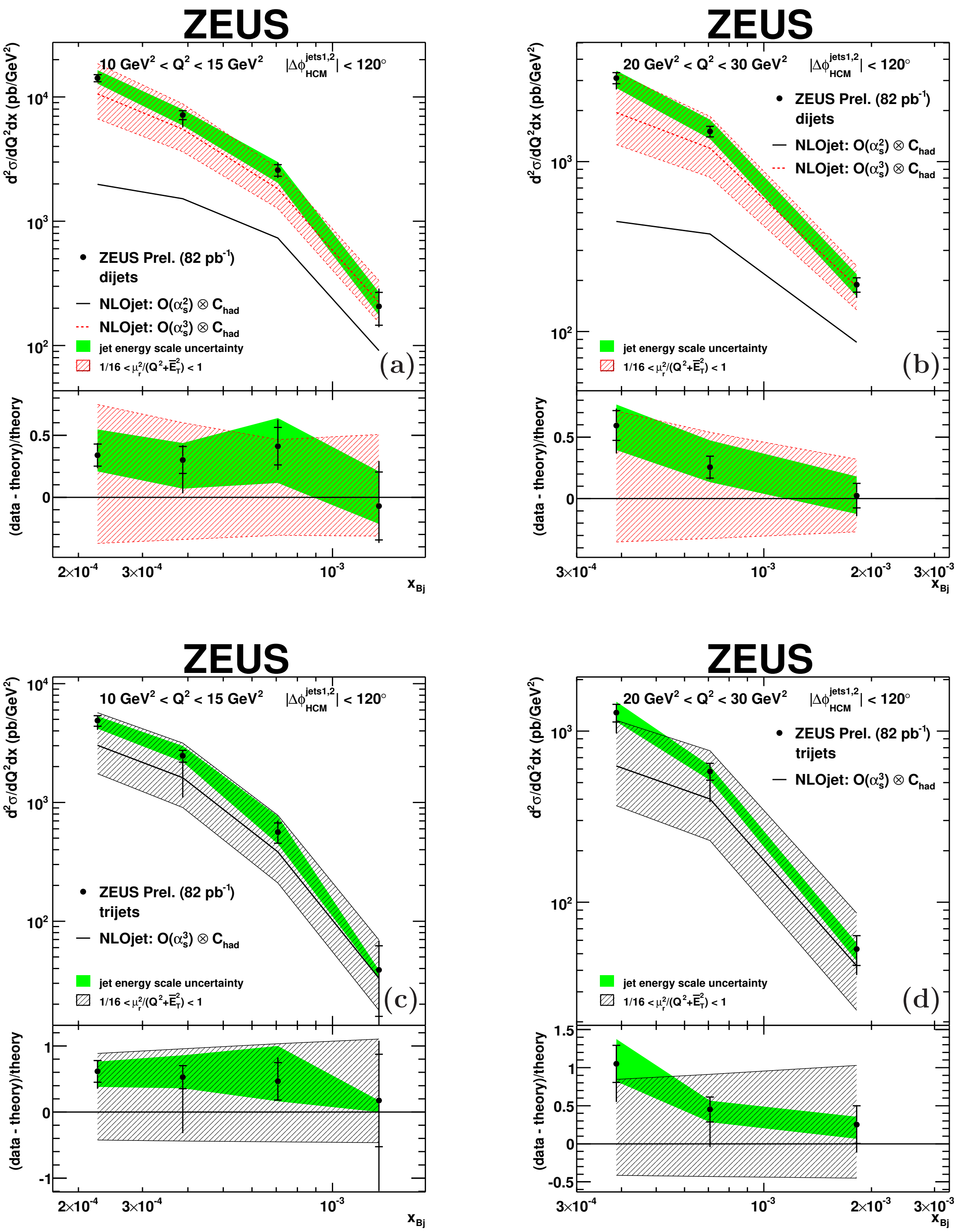

Figure 6: *The dijet and trijet cross sections for events with $\Delta\phi^{\rm jet1,2}_{HCM} < 120^\circ$ as functions of x_{Bj} in two different Q^2-bins. For comparison with the dijet measurements,* NLOJET *calculations at $\mathcal{O}(\alpha_s^2)$ ($\mathcal{O}(\alpha_s^3)$) are shown as solid (dashed) lines. The trijet measurements are compared to* NLOJET *calculations at $\mathcal{O}(\alpha_s^3)$. Other details as in the caption to Fig. 1.*